

2013


# Real-Time in vivo Imaging of Size-Dependent Transport and Toxicity of Gold Nanoparticles in Zebrafish Embryos Using Single Nanoparticle Plasmonic Spectroscopy

Lauren M. Browning  
*Old Dominion University*

Tao Huang  
*Old Dominion University*

Xiao-Hong Nancy Xu  
*Old Dominion University, xhxu@odu.edu*

Follow this and additional works at: [https://digitalcommons.odu.edu/chemistry\\_fac\\_pubs](https://digitalcommons.odu.edu/chemistry_fac_pubs)

 Part of the [Biophysics Commons](#), [Biotechnology Commons](#), and the [Nanoscience and Nanotechnology Commons](#)

## Repository Citation

Browning, Lauren M.; Huang, Tao; and Xu, Xiao-Hong Nancy, "Real-Time in vivo Imaging of Size-Dependent Transport and Toxicity of Gold Nanoparticles in Zebrafish Embryos Using Single Nanoparticle Plasmonic Spectroscopy" (2013). *Chemistry & Biochemistry Faculty Publications*. 137.

[https://digitalcommons.odu.edu/chemistry\\_fac\\_pubs/137](https://digitalcommons.odu.edu/chemistry_fac_pubs/137)

## Original Publication Citation

Browning, L. M., Huang, T., & Xu, X. H. N. (2013). Real-time *in vivo* imaging of size-dependent transport and toxicity of gold nanoparticles in zebrafish embryos using single nanoparticle plasmonic spectroscopy. *Interface Focus*, 3(3), 14. doi:10.1098/rsfs.2012.0098



## Research

**Cite this article:** Browning LM, Huang T, Xu X-HN. 2013 Real-time *in vivo* imaging of size-dependent transport and toxicity of gold nanoparticles in zebrafish embryos using single nanoparticle plasmonic spectroscopy. *Interface Focus* 3: 20120098.

<http://dx.doi.org/10.1098/rsfs.2012.0098>

One contribution of 10 to a Theme Issue 'Molecular-, nano- and micro-devices for real-time *in vivo* sensing'.

### Subject Areas:

nanotechnology, biophysics

### Keywords:

*in vivo* imaging, *in vivo* assays, nanotoxicity, single nanoparticle imaging and diffusion, single nanoparticle plasmonic spectroscopy, zebrafish embryos

### Author for correspondence:

Xiao-Hong Nancy Xu

e-mail: [xhxu@odu.edu](mailto:xhxu@odu.edu)

# Real-time *in vivo* imaging of size-dependent transport and toxicity of gold nanoparticles in zebrafish embryos using single nanoparticle plasmonic spectroscopy

Lauren M. Browning, Tao Huang and Xiao-Hong Nancy Xu

Department of Chemistry and Biochemistry, Old Dominion University, Norfolk, VA 23529, USA

Noble metal nanoparticles (NPs) show distinctive plasmonic optical properties and superior photostability, enabling them to serve as photostable multi-coloured optical molecular probes and sensors for real-time *in vivo* imaging. To effectively study biological functions *in vivo*, it is essential that the NP probes are biocompatible and can be delivered into living organisms non-invasively. In this study, we have synthesized, purified and characterized stable (non-aggregated) gold (Au) NPs ( $86.2 \pm 10.8$  nm). We have developed dark-field single NP plasmonic microscopy and spectroscopy to study their transport into early developing zebrafish embryos (cleavage stage) and their effects on embryonic development in real-time at single NP resolution. We found that single Au NPs (75–97 nm) passively diffused into the embryos via their chorionic pore canals, and stayed inside the embryos throughout their entire development (120 h). The majority of embryos ( $96 \pm 3\%$ ) that were chronically incubated with the Au NPs (0–20 pM) for 120 h developed to normal zebrafish, while an insignificant percentage of embryos developed to deformed zebrafish ( $1 \pm 1\%$ ) or dead ( $3 \pm 3\%$ ). Interestingly, we did not observe dose-dependent effects of the Au NPs (0–20 pM) on embryonic development. By comparing with our previous studies of smaller Au NPs ( $11.6 \pm 0.9$  nm) and similar-sized Ag NPs ( $95.4 \pm 16.0$  nm), we found that the larger Au NPs are more biocompatible than the smaller Au NPs, while the similar-sized Ag NPs are much more toxic than Au NPs. This study offers *in vivo* assays and single NP microscopy and spectroscopy to characterize the biocompatibility and toxicity of single NPs, and new insights into the rational design of more biocompatible plasmonic NP imaging probes.

## 1. Introduction

Noble metal nanoparticles (NPs; e.g. Au and Ag NPs) show distinctive plasmonic optical properties, superior photostability and high quantum yields (QYs) of Rayleigh scattering [1–6]. The QY here refers to the ratio of the scattering intensity (number of scattering photons) of a single NP to the intensity of its incident light. The plasmonic optical properties of single NPs highly depend upon their sizes, shapes, dielectric constants, and surrounding environments [1–7]. We have used localized surface plasmon resonance (LSPR) spectra of single Au and Ag NPs to determine their sizes, shapes, surface properties, and surrounding environments at single NP resolution [7–20]. Unlike fluorescence molecules or quantum dots (QDs), single plasmonic NPs resist photobleaching and photoblinking, and can be imaged and characterized in single live cells and embryos for any desired period of time [7–21]. Thus, they are most suitable for the study of dynamic events of interest *in vivo* in real-time.

We have demonstrated that single Au and Ag NPs can serve as superior photostable optical molecular probes and sensors for imaging of single live cells and embryos *in situ* and in real-time, using dark-field optical microscopy

and spectroscopy (DFOMS) [7–21]. Unlike any other imaging tools, such as transmission electron microscopy (TEM) or scanning probe microscopy, DFOMS offers high temporal resolution and throughput to trace, quantify and characterize multiple individual NPs *in vivo* in real-time simultaneously [11,13,16,18,19]. We have recently developed photostable optical nanoscopy (PHOTON) and single molecule nanoparticle optical biosensors, which enable DFOMS to image single molecules and single NPs at millisecond (ms) temporal and nanometre spatial resolutions [17,22].

To serve as effective imaging probes and sensors for the study of biological functions in living organisms, it is essential that these plasmonic NP probes are biocompatible and can penetrate living organisms on their own (non-invasively). Despite extensive study of Au NPs and their potential applications in biology and medicine [23,24], their effects on living organisms and their dependence upon physicochemical properties of the NPs still remain largely unknown [25–28].

Currently, *in vitro* studies account for the majority of nanotoxicity research [25–28]. However, the results from *in vitro* studies can be misleading. For example, *in vitro* assays may not capture critical insights into the effects of NPs upon intercellular functions and their related biological functions *in vivo*. Certain nanomaterials may interfere with the readout of common cytotoxicity assays because of their interactions with assay reagents, and their overlapping absorption, scattering or emission properties. A wide range of NP concentrations, exposure times, cell lines, and cell culture conditions have been used among various *in vitro* studies, which make direct comparison among the studies extremely difficult [25–28]. Furthermore, many studies used unpurified and unstable (aggregated) NPs, or the NPs coated with different surface functional groups, and these studies did not consider the potential toxic effects of surface functional groups, aggregations of NPs, and other contaminant chemicals (impurities) on the cells. The majority of studies did not characterize the physical properties (e.g. sizes, doses) of NPs throughout the entire duration of experiments *in situ* in real-time. Thus, various studies created a wide range of inconclusive, contradictory or misleading results.

To overcome the limitations of current nanotoxicity studies, we have developed ultrasensitive *in vivo* assays (cleavage-stage zebrafish embryos) to characterize the biocompatibility and toxicity of nanomaterials [11,16,18,19]. To depict the dependence of NP toxicity on their physicochemical properties, and to rationally design biocompatible NP imaging probes, we have synthesized a mini-library of Au and Ag NPs with various sizes and surface functional groups, purified them, determined their stability, and developed DFOMS to characterize them throughout their incubation with living organisms *in situ* in real-time at single NP resolution [7–21].

Zebrafish (*Danio rerio*) have served as an effective model organism to study human disease, development and physiology, and to assess potential drug toxicity [29–32]. They are superior to other model organisms (e.g. mouse, rat, human) [29–32]. For instance, zebrafish develop *ex utero* and their embryos are optically transparent, which enables real-time visualization of the entire embryonic developmental processes *in vivo*. By 120 hours-post-fertilization (hpf), the embryos fully develop to larvae with discrete organs, which show anatomical and physiological similarity to their mammalian counterparts. A pair of zebrafish can produce massive amounts (200–300) of embryos overnight at a very

low cost. These superior characteristics enable zebrafish embryos to serve as *in vivo* high-throughput assays to study the biocompatibility and toxicity of nanomaterials [11,16,18,19].

In our previous studies, we used cleavage-stage zebrafish embryos to study the transport, biocompatibility and toxicity of purified Ag NPs with three distinctive sizes ( $11.6 \pm 3.5$ ,  $41.6 \pm 9.1$  and  $95.4 \pm 16.0$  nm) and the smaller Au NPs ( $11.6 \pm 0.9$  nm) [11,16,18,19]. In this study, we use zebrafish embryos to characterize the transport, biocompatibility and toxicity of the larger Au NPs ( $86.2 \pm 10.8$  nm), aiming to determine the dependence of the biocompatibility and toxicity of the NPs upon their sizes and chemical compositions for rational design of biocompatible NP probes.

## 2. Results and discussion

### 2.1. Synthesis and characterization of purified and stable Au NPs ( $86.2 \pm 10.8$ nm)

We synthesized the Au NPs ( $86.2 \pm 10.8$  nm) by reducing HAuCl<sub>4</sub> with sodium citrate, as described in Materials and methods [33–35]. The colloidal Au NPs were thoroughly washed three times using centrifugation to remove any trace chemicals from the synthesis to prepare highly purified Au NPs. We suspended purified Au NPs in egg water (1.0 mM NaCl in deionized (DI) water; embryonic medium) and characterized their sizes, plasmonic optical properties and concentration in egg water over the entire embryonic development (120 h) using high-resolution TEM, dynamic light scattering (DLS), DFOMS and UV–vis absorption spectroscopy, respectively.

The TEM images and histograms of size distributions of single Au NPs (figure 1A,B) show the average sizes of ( $85.4 \pm 11.6$ ) and ( $86.2 \pm 10.8$ ) nm of the ellipse-shaped NPs dispersed in egg water at 0 and 120 h, respectively. The results show that the sizes of the NPs remain essentially unchanged over their 120 h incubation with egg water. The average sizes of NPs are calculated by averaging the length and width of each NP. The aspect ratios of the ellipse-shaped NPs range from 0.9 to 3.8, which are calculated by dividing the length of the NP by its width.

We also characterize the sizes of Au NPs in egg water over 120 h using DLS. The results (figure 1C) show their average sizes (diameters) of ( $86.3 \pm 9.0$ ) and ( $87.9 \pm 9.4$ ) nm at 0 and 120 h, indicating that the sizes of the NPs remain essentially unchanged and that the NPs are very stable (non-aggregated) over their 120 h incubation with egg water. Unlike TEM, which measures the sizes of individual NPs, DLS offers ensemble measurement of the average sizes of NPs dispersed in egg water. The sizes of hydrated NPs measured using DLS (figure 1C) are slightly larger than those measured by TEM (figure 1A,B). Furthermore, the sizes of the ellipse-shaped NPs determined by DLS are calculated using equations for spherical NPs, which approximate the ellipse-shaped NPs as spherical ones. They are not presented as the average of length and width of each ellipse-shaped NP as we calculated the sizes of the NPs determined by TEM. Thus, one cannot directly compare the hydrated ellipse-shaped NPs measured by DLS with their sizes determined by TEM and calculated as the average of their lengths and widths. Nonetheless, the sizes of NPs determined by both DLS and TEM are quite close, indicating that the approximation of ellipse-shaped NPs as spherical NPs for ensemble DLS measurement is

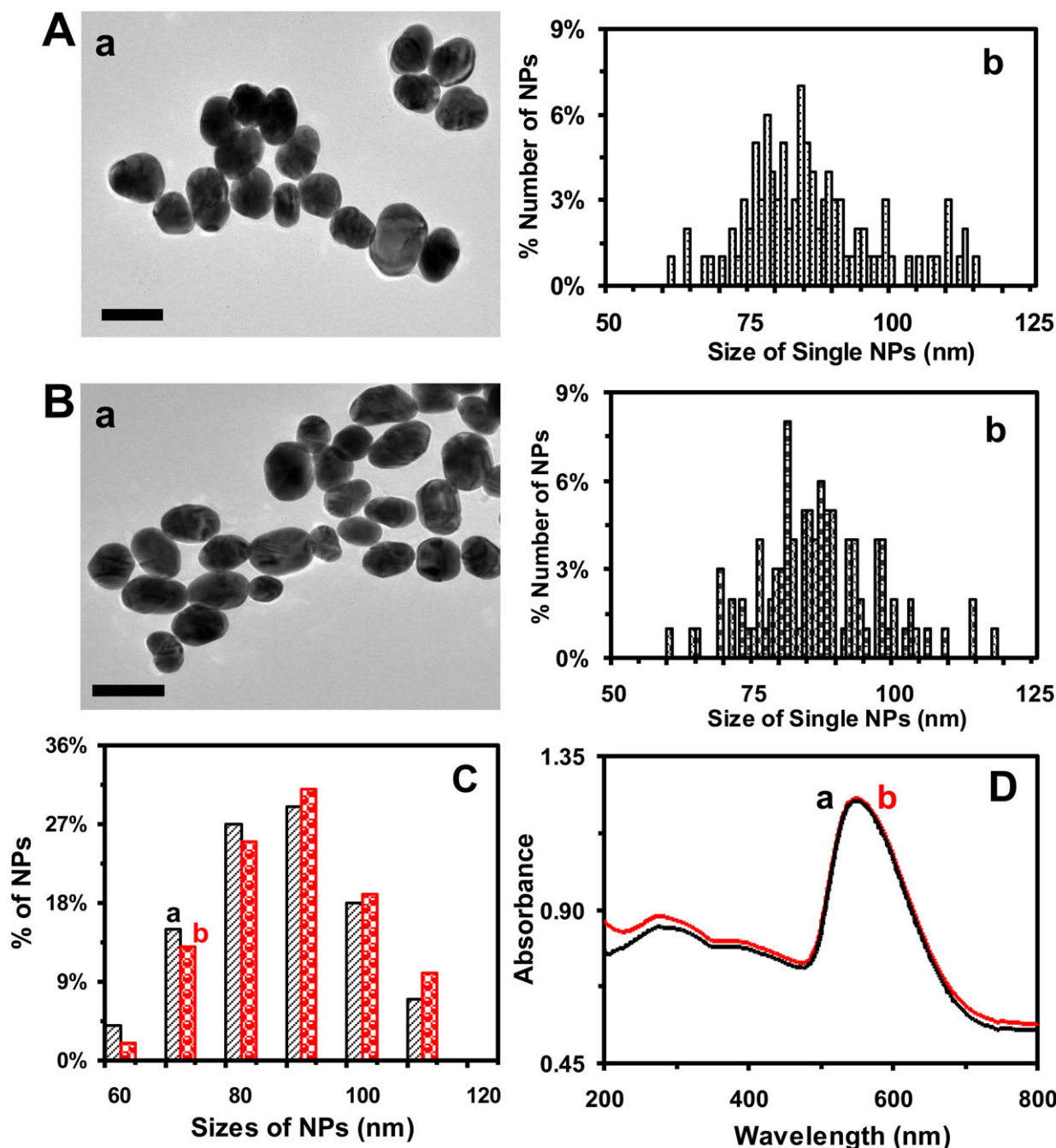


**Figure 1.** Characterization of sizes and stability (non-aggregation) of the Au NPs suspended in egg water (20 pM) at 28.5°C over 120 h. (A,B): (a) High-resolution TEM images of the Au NPs that had been suspended in egg water for: (A) 0 and (B) 120 h, showing single ellipse-shaped NPs. (b) Histograms of the size distributions of single Au NPs measured by high-resolution TEM show average sizes of NPs: (A)  $(85.4 \pm 11.6)$  and (B)  $(86.2 \pm 10.8)$  nm. Sizes are calculated by averaging the length and width of each NP, and their aspect ratios range from 0.9 to 3.8. (C) Histograms of size distributions of the NPs dispersed in egg water and measured by DLS show that their average sizes are (a)  $(86.3 \pm 9.0)$  and (b)  $(87.9 \pm 9.4)$  nm for 0 and 120 h, respectively. (D) UV-vis absorption spectra of the Au NPs in (C) at: (a) 0 and (b) 120 h, showing that the  $\lambda_{\max}$  (FWHM) at 550 ( $102 \pm 4$ ) nm remains unchanged over time. Scale bars in (A,B) are 100 nm.

acceptable. In this study, we use the sizes of the NPs determined by TEM to describe the sizes of the NPs.

We also study the concentrations and stability of the Au NPs in egg water over 120 h by measuring their UV-vis absorption spectroscopy (ensemble measurements). The absorption spectra of the NPs in egg water (20 pM) over 120 h show that their baseline subtracted peak absorbance of 0.53 at 550 nm,  $\lambda_{\max}$  (full width at half maximum, FWHM =  $102 \pm 4$  nm), remains unchanged (figure 1D), which further demonstrates that the Au NPs are stable in egg water over 120 h. If the NPs were aggregated (unstable), the absorbance of their UV-vis absorption spectra would decrease and their peak wavelength would be red shifted. But that was not what

we observed. Thus, the NPs remain stable (non-aggregated) in egg water over 120 h.

We further characterize plasmonic optical properties of single Au NPs and their stability in egg water over 120 h at single NP resolution using DFOMS. Dark-field optical images of single Au NPs and histograms of distributions of plasmonic colours (LSPR spectra of single NPs) show that the majority of single NPs exhibit plasmonic green with some being orange and red, which remains essentially unchanged over their 120 h incubation with egg water (figure 2A–C). We determine the number of single NPs in egg water (concentrations at single NP resolution) over 120 h using DFOMS. Unlike UV-vis spectroscopy (ensemble measurement), DFOMS enables us to image

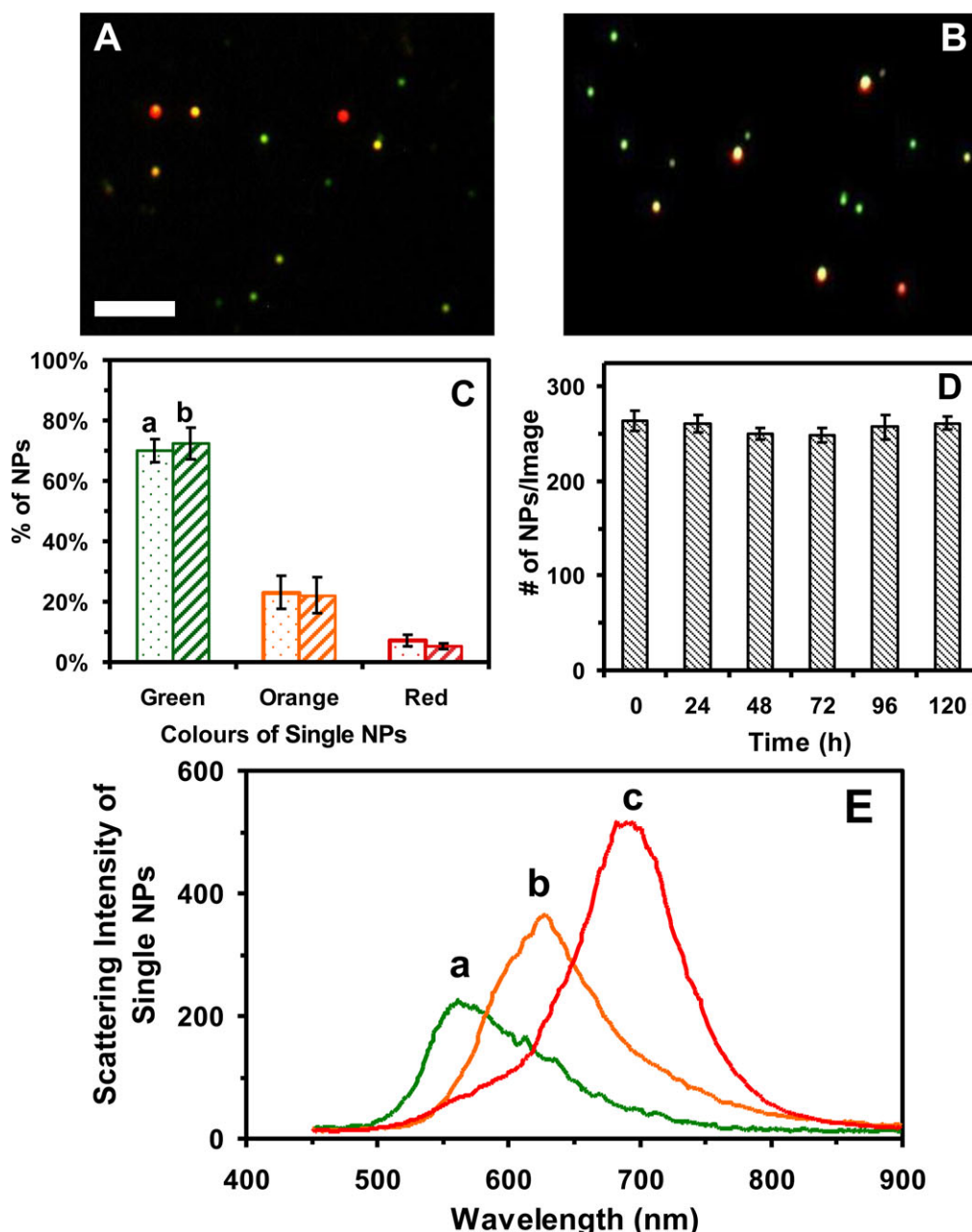


**Figure 2.** Characterization of the plasmonic optical properties and stability (non-aggregation) of single Au NPs suspended in egg water (20 pM) at 28.5°C over 120 h. (A,B) Dark-field optical images of the Au NPs that had been suspended in egg water for: (A) 0 and (B) 120 h, showing single plasmonic green, orange and red NPs. (C) Histograms of colour distributions of the single Au NPs in (A,B) measured by DFOMS show: (a)  $(70 \pm 4)\%$  of plasmonic green,  $(23 \pm 5)\%$  of orange and  $(7 \pm 2)\%$  of red NPs; and (b)  $(72 \pm 5)\%$  of plasmonic green,  $(22 \pm 6)\%$  of orange and  $(5 \pm 1)\%$  of red NPs. (D) The number of single Au NPs imaged by DFOMS (similar to those zoom-in images in A,B) is  $264 \pm 10$ ,  $261 \pm 9$ ,  $250 \pm 6$ ,  $249 \pm 8$ ,  $257 \pm 13$ , and  $261 \pm 7$  NPs per image at 0, 24, 48, 72, 96, and 120 h, respectively, indicating that the number of NPs remains unchanged over time, and that the NPs are stable in egg water over 120 h. (E) Representative LSPR spectra of single plasmonic green, orange and red Au NPs show  $\lambda_{\max}$  (FWHM) at: (a) 554 (105); (b) 619 (97); (c) 683 (82) nm. The scale bars in (A,B) are 2  $\mu\text{m}$ , which show the distances between individual NPs, but not their sizes because of the optical diffraction limit.

the number of single NPs in a given detection volume (one full-frame charge-coupled device (CCD) image) to determine the concentration of NPs at single NP resolution. The number of single NPs (20 pM Au NPs) in 60 images acquired by DFOMS at each given incubation time is  $(257 \pm 2)$  NPs per image (figure 2D), demonstrating that the NPs in egg water are very stable (non-aggregated). If the NPs were aggregated (unstable), their number in solution would have decreased over time. But that was not what we observed. Thus, the NPs remain stable (non-aggregated) in egg water over 120 h. As we reported previously [20], DFOMS is a much more sensitive, accurate and direct method to determine the concentrations and plasmonic optical properties of single NPs than UV-vis

absorption spectroscopy. Representative LSPR spectra of single Au NPs in egg water (figure 2E) show peak wavelengths ( $\lambda_{\max}$ ) with FWHM,  $\lambda_{\max}$  (FWHM), at 554 (105), 619 (97) and 683 (82) nm, which remain essentially unchanged over 120 h. The ellipse-shaped NPs with aspect ratios up to 3.8 and rough surfaces, as shown in TEM images (figure 1A,B), make the LSPR of the NPs red shifted.

We characterize the stability of a dilution series of the purified Au NPs using the above approaches, to determine their 'solubility' (a maximum concentration) that the Au NPs are stable in egg water over 120 h. We then use the concentrations of the stable and 'soluble' (non-aggregated) Au NPs in egg water to incubate with cleavage-stage embryos,

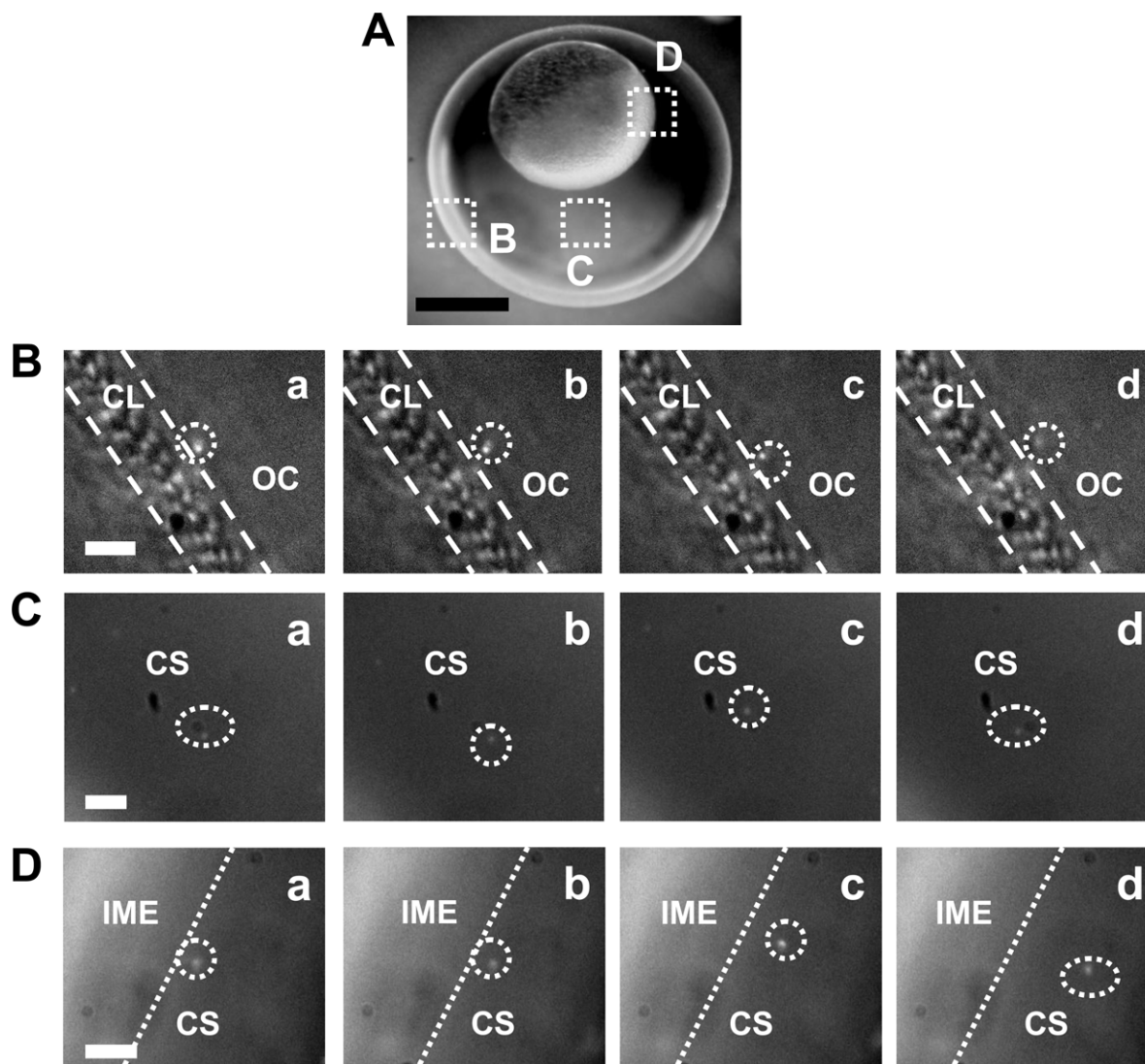


**Figure 3.** Real-time imaging of transport of single Au NPs ( $86.2 \pm 10.8$  nm; 20 pM) into cleavage-stage zebrafish embryos using DFOMS. (A) Optical image of the cleavage-stage embryo in egg water shows its chorionic layer (CL), chorionic space (CS) and the interface of the CS and the inner mass of the embryo (IME), as highlighted by (B–D), respectively. (B–D) Snapshots of sequential dark-field optical images of the zoom-in areas squared in (A) show the diffusion of single Au NPs (circled) from the egg water (outside chorion, OC) into the CL, in the CS, and at the interface between the CS and IME, respectively. The temporal resolution of real-time imaging is 100 ms. Scale bars are: (A) 200 and (B–D) 5  $\mu$ m.

follow embryonic development over 120 h, and study the effects of NPs on embryonic development. Unlike other studies, we use DFOMS to characterize the stability (LSPR spectra and number) of Au NPs in egg water at single NP resolution *in situ* in real-time, which is much more sensitive and accurate than any conventional ensemble measurements (e.g. UV–vis absorption spectroscopy).

We correlate the distribution of sizes of single Au NPs measured by TEM with the distribution of plasmonic colours (LSPR spectra) of single Au NPs in egg water determined by DFOMS. At 120 h, the results from TEM measurements show that the sample includes 63% of 60–88 nm, 28% of 89–100 nm and 9% of 101–118 nm NPs (figure 1B). Dark-field optical imaging of single Au NPs (figure 2C-b) shows that a majority of single NPs exhibit plasmonic green ( $65 \pm 4$ )% with some being orange ( $28 \pm 1$ )% and red ( $7 \pm 3$ )%. Note that TEM samples are prepared from the same Au NP solutions as those measured by DFOMS. Thus, for this Au NP solution, the NPs with sizes of 60–88, 89–100 and 101–118 nm show plasmonic green, orange and red, respectively. Using such simple calibration approaches (colours-as-size

index) as we reported previously [7,12,14–16,36], we can determine the sizes of single Au NPs *in situ* in real-time at nanometre resolution using their LSPR spectra via DFOMS.

Taken together, the results in figures 1 and 2 show that the Au NPs (20 pM) are very stable (non-aggregated) in egg water over the entire duration of embryonic development (120 h), which enables us to study their size- and dose-dependent transport into/in embryos and their effects on embryonic development *in vivo* in real-time. If the NPs were unstable (aggregated), their number in solution would have decreased, and their sizes would have increased over time, which would have made the study of dose- and size-dependent nanotoxicity unreliable.

## 2.2. Analysis and characterization of molar concentrations of the Au NPs

We used molar concentrations of single Au NPs (but not atoms or ions) to describe dose-dependent nanotoxicity. We calculated their molar concentrations by dividing moles of single Au NPs by the solution volume, and characterized

them as we described previously [11,16,18,19,35]. Briefly, we calculated the weight of Au ( $W_{\text{Au}}$ ) generated by the complete reduction of  $\text{HAuCl}_4$  by multiplying the moles of added  $\text{HAuCl}_4$  by the atomic weight of Au ( $196.967 \text{ g mol}^{-1}$ ). The volume of generated Au ( $V_{\text{Au}}$ ) was determined by dividing  $W_{\text{Au}}$  by the density of Au ( $d = 19.3 \text{ g cm}^{-3}$ ). The number of Au NPs, diameter ( $\text{Dia}$ ) =  $86.2 \pm 10.8 \text{ nm}$ , was computed by dividing the volume of generated Au ( $V_{\text{Au}}$ ) by the volume of one NP. The moles of Au NPs were then determined by dividing the number of Au NPs by Avogadro's constant ( $6.02 \times 10^{23}$ ). Finally, the molar concentrations of Au NPs were calculated by dividing the moles of Au NPs by the solution volume.

We measured UV-vis absorption spectra of a dilution series of unwashed Au NP solutions, determined the baseline subtracted peak absorbance and plotted the subtracted peak absorbance versus molar concentrations of NPs to determine their molar absorptivity (extinction coefficient,  $\epsilon_{550 \text{ nm}}$ ) at a peak wavelength ( $\lambda_{\text{max}} = 550 \text{ nm}$ ) of  $2.7 \times 10^{10} \text{ M}^{-1} \text{ cm}^{-1}$ , which agrees excellently with those measured previously for similar-sized Au NPs [35].

The NPs were spun down using centrifugation to remove the by-products of the reaction and any excess of chemicals in solution. The NPs in the pellets were fully resuspended in DI water to produce the first-time washed NP solution. We characterized the sizes of NPs using DLS and UV-vis spectroscopy, which showed that their sizes,  $\lambda_{\text{max}}$  and  $\epsilon_{550 \text{ nm}}$  remained unchanged. Using the same approaches, we found that the sizes,  $\lambda_{\text{max}}$  and  $\epsilon_{550 \text{ nm}}$  of the second- and third-washed Au NPs remained unchanged.

We imaged and determined any potential trace amount of individual Au NPs in the supernatants collected from washing of the Au NPs using DFOMS. If any Au NPs were present in the supernatant, we would further remove them from the supernatant using ultra-centrifugation (L90, Beckman). The supernatants from the last washing of the NPs, which contain any residual chemicals except Au NPs, were collected and used to treat embryos. The experiments served as controls for the study of the effects of potential residual chemicals on embryonic development.

Note that the weight and surface area of single NPs are proportional to the number (mole) of single NPs. Thus, the molar concentration of NPs accurately represents the size, number (mole) and surface properties of the NPs. Therefore, the dose-dependent effects of NPs on embryonic development in molar concentrations represent the dependence of nanotoxicity on their sizes, number and surface properties. By contrast, the  $w/v$  (weight/volume) concentrations of NPs cannot represent the number (doses) of NPs, and cannot accurately reflect the dependence of nanotoxicity on the number and surface properties of the NPs, because the different-sized NPs with the same  $w/v$  concentration contain a different number of NPs, and thus different surface areas and charges of the NPs.

### 2.3. Real-time imaging of transport of the single Au NPs into/in embryos

We incubated the purified and stable Au NPs (20 pM) with the cleavage-stage zebrafish embryos and imaged the diffusion and transport of single NPs into the embryos and inside the embryos *in vivo* in real-time, aiming to determine whether such larger Au NPs (60–118 nm) can transport into living embryos and their transport mechanism. The snapshots of

sequential optical images (figure 3) show arrays of chorionic pores on chorionic layers (CLs) and their diameters (0.5–0.7  $\mu\text{m}$ ) and that single Au NPs diffuse through the chorionic pore canals into the chorionic space (CS), and through the CS into the inner mass of the embryos (IME). We characterized the LSPR spectra of single Au NPs, such as those shown in figure 2E, to distinguish single Au NPs over embryonic tissues and debris, which appear white under dark-field illumination.

Representative diffusion trajectories of single Au NPs (figure 4a), each with an identical green colour (size), show that single Au NPs are diffusing (A) into the embryo via chorionic pores; (B) in the CS; and (C) into the IME from the CS. The diffusion modes of these single Au NPs in various locations of the developing embryos are further characterized by plotting real-time square displacement (RTSD) of single Au NPs versus diffusion time (figure 4b). Note that viscosities inside a developing embryo vary widely upon local embryonic environments, which also alter rapidly with time as the embryo develops. Therefore, we use RTSD (diffusion distance at each time interval) instead of MSD (mean-square displacement, average distance over time) to determine the diffusion modes and diffusion coefficients of single NPs, as they diffuse into and through embryos.

Using diffusion theories [37–39], we found restricted diffusion for the NPs that diffused from egg water through the chorionic pores into the CS (figure 4A–b). Several steps in the plot suggest that the NPs become trapped (2–8 s) within the pores from time to time, possibly because of their interactions with the pores. Nonetheless, the linear plot shows stationary random Brownian diffusion as a diffusion mode for the NPs entering into the embryos. Thus, passive diffusion, but not active transport, is responsible for the NPs entering the embryos. The diffusion coefficients ( $D$ ) are determined by dividing the slope of the plot of RTSD versus time by 4 using two-dimension random walk theory ( $\text{RTSD} = 4D\Delta t$ ). The diffusion coefficients vary drastically as the NPs diffuse from the egg water through the chorionic pores and into the CS with an average of  $(1.7 \pm 1.5) \times 10^{-9} \text{ cm}^2 \text{ s}^{-1}$ . Their larger standard deviation reflects highly heterogeneous embryonic environments.

The plots of RTSD versus time for single Au NPs that diffuse in the CS and from the CS into the IME also exhibit linearity with larger slopes and fewer steps (figure 4b in B,C), showing simple random Brownian diffusion and suggesting that the transport barrier at the CL is much higher than the interface of the CS and IME. Their average diffusion coefficients in (B) and (C) are  $(6.3 \pm 2.7) \times 10^{-9}$  and  $(5.1 \pm 2.1) \times 10^{-9} \text{ cm}^2 \text{ s}^{-1}$ , respectively. Notably, the slopes of the plots in (C) change over time much more notably and they are smaller than those in (B), suggesting higher viscosity gradients at the interface of the CS and IME than those in the CS.

We use the same approaches to study the diffusion of plasmonic green Au NPs in egg water, which shows random Brownian diffusion with diffusion coefficients of  $(1.6 \pm 0.2) \times 10^{-8}$ . Note that diffusion coefficients of single NPs are inversely proportional to the viscosity of the medium, as described by the Stokes–Einstein equation,  $D = kT/(6\pi\eta a)$ , for a spherical NP, where  $k$  is the Boltzmann constant;  $T$  is the temperature;  $a$  is the radii of single NPs; and  $\eta$  is the viscosity of the medium where NPs diffuse in [40]. Thus, the results show that embryonic environments are orders of magnitude more viscous than egg water. These results agree well with those we reported previously using similar-sized Ag NPs [19],

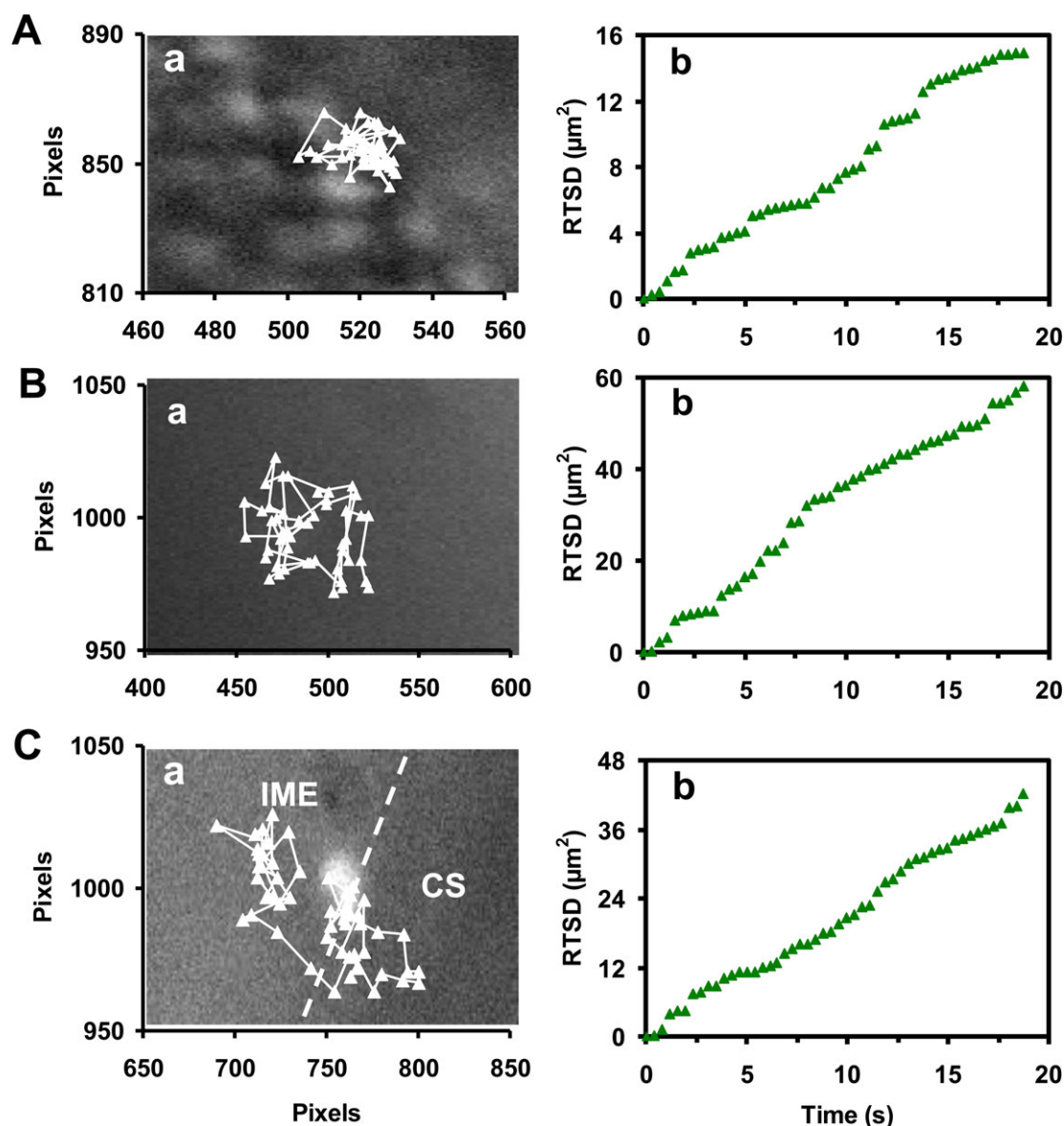


**Figure 4.** Real-time study of the diffusion modes of single Au NPs in cleavage-stage embryos. (a) Diffusion trajectories and (b) plots of real-time square displacement (RTSD) versus time of single plasmonic green Au NPs that diffuse: (A) from the egg water into the CS; (B) in the CS; and (C) at the interface between the CS and IME (as shown in figure 3) indicate restricted diffusion in (A) and random Brownian motion in (B,C) with diffusion coefficients of  $(1.7 \pm 1.5) \times 10^{-9}$ ,  $(6.3 \pm 2.7) \times 10^{-9}$  and  $(5.1 \pm 2.1) \times 10^{-9} \text{ cm}^2 \text{ s}^{-1}$ , respectively. The embryos were incubated with the Au NPs (20 pM) in egg water and imaged in real-time. Each pixel is 67 nm.

showing highly heterogeneous embryonic environments with larger viscosity gradients.

Taken together, the results in figure 4 show that the same-sized Au NPs diffuse 14.96, 58.36 and 42.44  $\mu\text{m}^2$  within the same duration of measurement (18.73 s) as the NPs diffuse across the CL, in the CS and into the IMS, suggesting the highest restriction at the CL and the lowest viscosity in the CS.

#### 2.4. Study of dose-dependent biocompatibility of the Au NPs ( $86.2 \pm 10.8 \text{ nm}$ )

To study the dose-dependent biocompatibility and toxicity of the Au NPs, we incubated the cleavage-stage embryos (0.75–2.25 hpf) with various concentrations (0–20 pM or 0–78  $\mu\text{g ml}^{-1}$ ) of the purified and stable Au NPs in egg water, and the supernatant collected from the last washing of the NPs over 120 h. We imaged the developing embryos every 24 h until they fully developed at 120 hpf. We characterized normally developed zebrafish (figure 5A), deformed

zebrafish (figure 5B) and dead embryos (figure 5C), using their morphologies and phenotypes. The percentage of embryos that developed to normal and deformed zebrafish or became dead was plotted against molar concentrations of the NPs and supernatants that were incubated with the embryos (figure 5D). The studies of embryonic development in the supernatant serve as control experiments to determine the effects of potential residual chemical contaminants on embryonic development, which ensure that the death and deformities of embryos exposed to the NPs are not caused by any potential residual chemicals from the NP synthesis.

This experimental design enables the NPs to passively diffuse into embryos without external intervention (non-invasively), allowing us to study their effects on embryonic development *in vivo* in real-time. These approaches also mimic the potential transport and effects of the NPs on aquatic and eco-living organisms should the NPs be released into the environment. We select the cleavage-stage embryos as *in vivo* assays to study the effects of NPs on embryonic



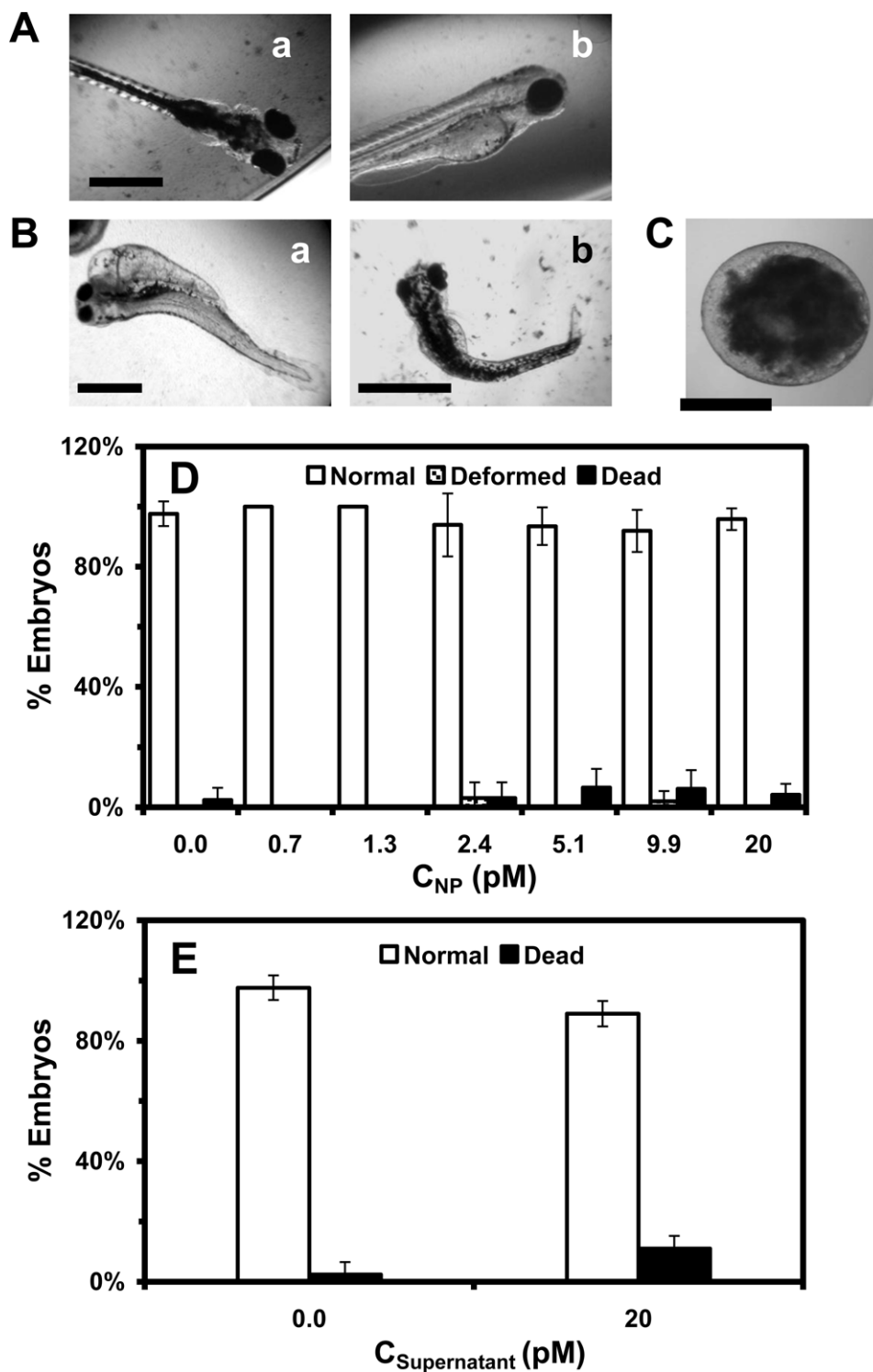


**Figure 5.** *In vivo* study of the effect of Au NPs on embryonic development. Optical images of: (A) normally developed zebrafish show normal development of the cardiac region, yolk sac, head and eyes; (B) deformed zebrafish display several deformities, including (a) finfold abnormality, tail/spinal cord flexure, cardiac malformation, yolk sac oedema and eye abnormality; and (b) finfold abnormality and tail/spinal cord flexure; and (C) dead embryo. (D) Histograms of the percentages of the embryos that developed to normal and deformed zebrafish or became dead versus NP concentration. (E) Control experiments: histograms of the percentages of embryos that developed to normal zebrafish or became dead either in egg water alone or in supernatant. A total of 48 embryos were studied for each NP concentration, and control. The percentages of embryos that developed to normal and deformed zebrafish or became dead are calculated by dividing each number by the total number of embryos used at each concentration. Their means and standard deviations (error bars) for each given concentration are calculated from triplicate measurements. Scale bars are: (A) 250, (B) 500 and (C) 200  $\mu\text{m}$ .

development because the embryonic cells at this stage synchronously divide and undergo molecular changes that ultimately affect the fates of developing embryos.

The results show that embryonic development insignificantly depends upon the NP concentration (dose) (figure 5D,E). As the NP concentration increases from 0 to 20 pM, the percentage

of embryos that develop into normal zebrafish remains essentially unchanged at  $(96 \pm 4)\%$ , and the numbers of embryos that develop into deformed zebrafish or became dead also remain the same at  $(1 \pm 1)\%$  and  $(3 \pm 3)\%$ , respectively. The statistical analysis of the data using ANOVA with a confidence level of 95% ( $p = 0.05$ ) reveals insignificant differences between

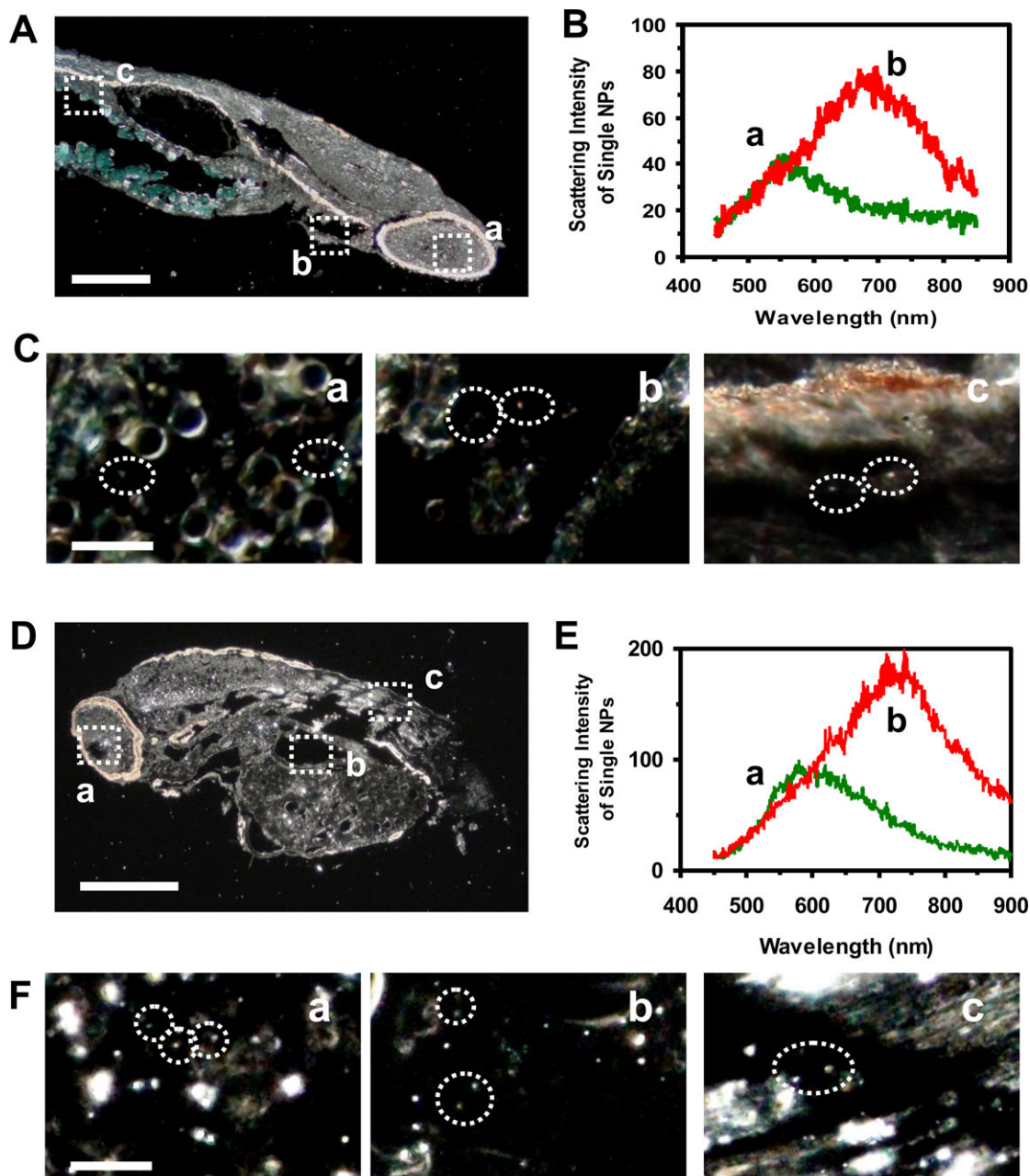


**Figure 6.** Quantitative imaging of single Au NPs embedded in (A–C) a normally developed zebrafish and (D–F) a deformed zebrafish using DFOMS. (A) Optical image of an ultrathin longitudinal section of a fixed zebrafish. The rectangles highlight its (a) retina (eye), (b) gill slits and (c) tail muscle. (B) LSPR spectra of single Au NPs embedded in the tissues show distinctive  $\lambda_{\max}$  (FWHM) at (a) 555 (157) and (b) 697 (174) nm. (C) Zoom-in optical images of those outlined in (A) show single Au NPs embedded in the tissues, as circled. (D) Optical image of an ultrathin longitudinal section of a fixed zebrafish that displayed multiple morphological abnormalities. The rectangles outline its (a) retina (eye), (b) yolk sac and (c) tail muscle. (E) LSPR spectra of single Au NPs embedded in the tissues show distinctive  $\lambda_{\max}$  (FWHM) at (a) 579 (186) and (b) 738 (194) nm. (F) Zoom-in optical images of those outlined in (D), show individual Au NPs embedded in the tissues, as circled. Scale bars are: (A,D) 200 and (C,F) 10  $\mu\text{m}$ .

dead and deformed embryos as they are exposed to various concentrations of Au NPs (0–20 pM), egg water or supernatant. Notably, the percentages of embryos that are incubated with the supernatant over 120 h and develop to normal zebrafish or become dead are the same as those in egg water alone (blank control) (figure 5E) and none of embryos develop to abnormal zebrafish, showing that the death and deformities observed in figure 5D are not caused by any potential residual chemicals from the NP synthesis.

The chronic treatment of embryos (48 embryos) with the Au NPs over 120 h results in only two abnormally developed zebrafish (figure 5B), which are rare events (the outliers) of the measurements and can only be detected at single embryo

resolution. Both of them display more than one type of deformation, and the types of deformation are independent of the NP concentration. For example, the embryo that has been incubated with the lower NP concentration (2.4 pM) for 120 h develops into the deformed zebrafish with all types of deformities (finfold abnormality, tail and spinal cord flexure, cardiac malformation, yolk sac oedema and eye abnormality). By contrast, the embryo that has been incubated with the higher NP concentration (9.9 pM) for 120 h develops into the deformed zebrafish with finfold abnormality and tail and spinal cord flexure. These observations suggest that some embryos may be more vulnerable (sensitive) to the effects of the Au NPs on their development, while other embryos may be more

tolerant (resistant) of the effects of the Au NPs. Notably, each embryo is quite distinctive, and it is common that a small percentage of the embryos become dead during development under the same incubation conditions (in egg water). Random diffusion of single Au NPs into the various compartments of the embryos, especially at such low concentrations, may also cause the rare and stochastic toxic effects on embryonic development, as we reported previously [16].

## 2.5. Quantitative imaging of single Au NPs in tissues of normal and deformed zebrafish

To determine why some embryos developed normally while others became deformed or dead, we imaged single Au NPs embedded in the tissues of normally developed and deformed zebrafish and quantitatively characterized distributions of single Au NPs in the tissues using DFOMS. We incubated the cleavage-stage embryos with the Au NPs (0–20 pM) continuously (chronically) for 120 h until they developed into normal or deformed zebrafish. We then rinsed and fixed the normally developed and deformed zebrafish and prepared ultrathin sections (1–4  $\mu\text{m}$  thickness) of their tissue samples as described in the Materials and methods. Individual Au NPs embedded in various tissues of normal and deformed zebrafish were characterized using DFOMS.

We observed the green, orange and red Au NPs embedded in different locations of normally developed zebrafish (figure 6A–C), including (a) retina, (b) gill slits and (c) tail muscles. The LSPR spectra of single Au NPs embedded in the tissues (figure 6B) show characteristic plasmonic peak wavelengths ( $\lambda_{\text{max}}$ ) at 555 nm (green) and 697 nm (red), enabling us to distinguish the Au NPs from the tissues. Single Au NPs were also observed in different locations of a deformed zebrafish (figure 6D–F), including (a) retina, (b) yolk sac and (c) tail muscles. LSPR spectra of single Au NPs embedded in the tissues (figure 6E) show distinctive peak wavelengths ( $\lambda_{\text{max}}$ ) at 579 nm (green) and 738 nm (red). These results suggest that the NPs diffuse into the developing embryo (figures 3 and 4) and remain inside the embryos throughout their developmental stages (120 h). The red shift of the LSPR spectra of single Au NPs could be attributed to the embryonic tissues, which decrease the surface refractive index of the NPs and offer lower dielectric constants than the egg water. Nonetheless, the potential aggregation of a very few single Au NPs embedded in the tissues during their incubation with embryos over 120 h could also lead to larger NPs and red shift of their LSPR spectra.

We quantitatively analysed the number and sizes of individual Au NPs embedded in the tissues using their distinctive plasmonic optical properties (colours, LSPR spectra), and size-dependent LSPR spectra. Unlike a conventional spectrograph that acquires LSPR spectra of single NPs one at a time, the DFOMS in this study is equipped with a multi-spectral imaging system (MSIS), which enables us to simultaneously acquire LSPR spectra of a massive number of single NPs, and to achieve high-throughput quantitative analysis of individual Au NPs embedded in the tissues of interest with both spatial and temporal resolutions.

Plots of the number of given plasmonic colours (sizes) of single NPs in normal and deformed zebrafish show that more NPs are embedded in the eye and tail tissues of the deformed zebrafish than in those of the normal zebrafish (figure 7). The percentages of plasmonic green and red NPs embedded in the tissues are similar to those observed in solution

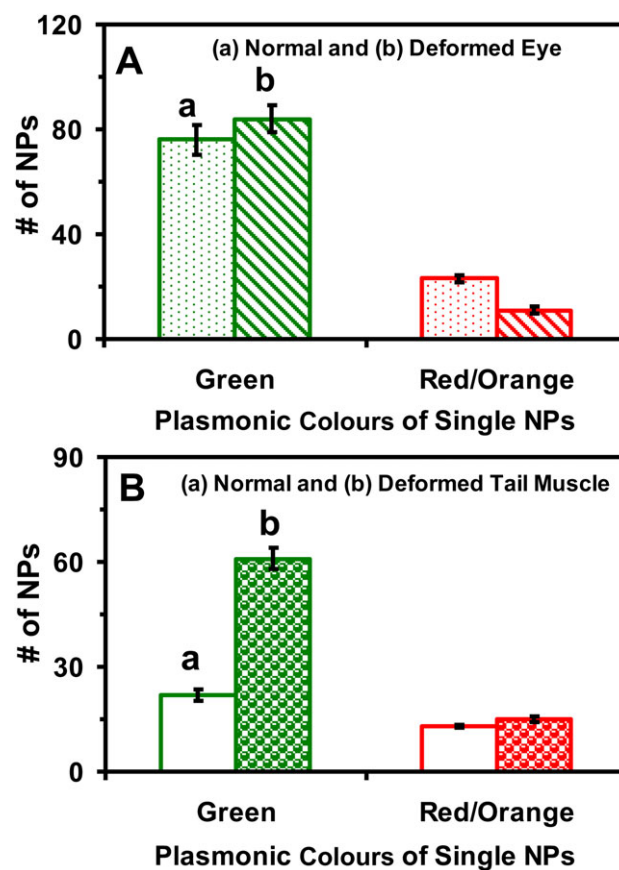


**Figure 7.** Quantitative analysis of the number and sizes of single Au NPs embedded in the tissues of normal and deformed zebrafish. Histograms of the number and sizes (colours) of single NPs embedded in (A) retina (eye) and (B) tail muscle of (a) normal and (b) deformed zebrafish. A minimum of three slices of each type of tissues were characterized for each analysis. The means and standard deviations (error bars) of each given type (plasmonic green and orange/red) of the Au NPs are calculated from each three replicated measurements.

(figure 2), which suggests that the NPs remain stable (non-aggregated) throughout their incubation with embryos in egg water over 120 h. The larger number of Au NPs accumulated inside the embryos throughout their development may lead to their deformation and death. Nonetheless, individual embryos might have various degrees of tolerance to the effects of the Au NPs. Embryos with a high degree of tolerance could survive and develop to normal zebrafish. By contrast, those with a low degree of tolerance could develop into deformed zebrafish or become dead.

Such individuality phenomena could not be detected if ensemble measurements were utilized. Therefore, this study further underscores the importance of studying the effects of the NPs on embryonic development at single NP and single embryo resolutions. The results further suggest that random walk of single Au NPs into/in embryos might have caused stochastic toxic effects on embryonic development, as those we reported previously [16].

## 2.6. Comparing with our previous studies: size- and chemical-dependent toxicity of Au and Ag NPs

To compare with our previous study of the effects of smaller Au NPs ( $11.6 \pm 0.9$  nm; 0–1.2 nM) on the embryonic

development [16], we plot the percentages of embryos that developed into normal or deformed zebrafish versus the surface area of Au NPs in a given solution volume (figure 8). The surface areas of two different-sized Au NPs are used to enable a full-scale comparison. The results show dose-independent effects of both smaller and larger Au NPs upon embryonic development. Interestingly, the results clearly reveal size-dependent biocompatibility and toxicity of Au NPs upon embryonic development. The larger Au NPs cause fewer embryos to become dead than the smaller Au NPs, suggesting that the larger Au NPs ( $86.2 \pm 10.8$  nm) are more biocompatible (less toxic) than smaller Au NPs ( $11.6 \pm 0.9$  nm) at the same given doses.

By contrast, our previous studies of the effects of purified and stable Ag NPs ( $11.6 \pm 3.5$ ,  $41.6 \pm 9.1$  and  $95.4 \pm 16.0$  nm with similar doses to the Au NPs) on the embryonic development show much higher toxicity of Ag NPs than the Au NPs [11,18,19]. The toxicity of Ag NPs highly depends on their doses and sizes [11,18,19]. For the same-sized Ag NPs, higher doses of Ag NPs cause more embryos to become dead or to develop into more severely deformed zebrafish. For the same doses of Ag NPs, the larger Ag NPs cause more embryos to become dead and to develop into more severely deformed zebrafish than smaller ones.

By comparing with these previous studies of smaller Au NPs and various-sized Ag NPs [11,16,18,19], we found the size-dependent and chemical-dependent biocompatibility and toxicity of the Au and Ag NPs. Notably, our previous studies neither predict nor conclude the effects of larger Au NPs ( $86.2 \pm 10.6$  nm) on the embryonic development. It is entirely unknown whether such larger Au NPs can be stable in egg water, whether they can enter the embryos and whether they are more biocompatible or toxic than the smaller Au or Ag NPs. Thus, all findings from this study are distinctive and cannot be extrapolated from any previous studies. In this study, we use exactly the same approaches (e.g. same stage of embryos, same exposure conditions and same characterization methods) as those used in the previous studies, except different-sized Au NPs. Such approaches are essential for us to determine the biocompatibility and toxicity of the NPs upon their sizes and chemical properties.

The molecular mechanisms of the size- and chemical-dependent effects of Au and Ag NPs upon embryonic development are currently under investigation. It is most likely that physico-chemical properties of the NPs, including their surface properties, sizes, shapes, doses, and chemical compositions, create combined and complex effects on embryonic development, and each physicochemical property could create distinctive effects on embryonic development at a given condition. For example, various sizes of NPs could potentially create different effects on molecular interactions (e.g. protein-protein interactions) and molecular transport in living organisms and alter their physico-chemical properties and nanoenvironments differently (e.g. charge, viscosity, stress, and diffusion of small molecules inside living organisms). Such effects may not be proportional to the sizes of the NPs, and may well depend upon the surface properties and chemical reactivity of the NPs. These effects could be dependent upon living organisms as well. Thus, it is important to study the effects of each physicochemical property of the NPs on a given living organism (e.g. cleavage-stage embryos) one at a

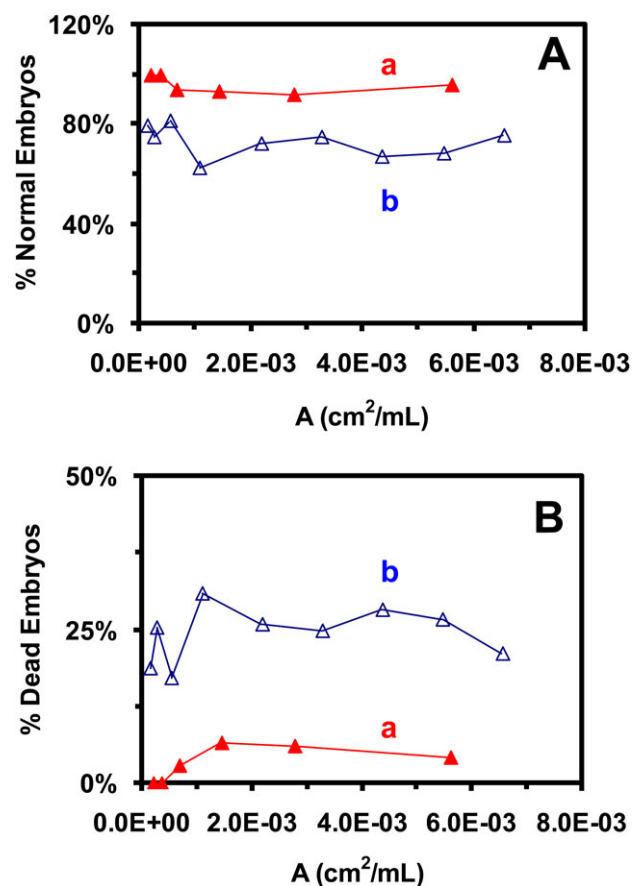


**Figure 8.** Study of size-dependent biocompatibility and toxicity of Au NPs on embryonic development. Percentages of embryos that were incubated with given concentrations of NPs in egg water for 120 h (A) developed to normal zebrafish or (B) became dead, versus the surface area of NPs per a given volume (dose) for: (a: filled triangles)  $86.2 \pm 10.8$  nm (this study; 0–20 pM); and (b: open triangles)  $11.6 \pm 0.9$  nm (previous study; 0–1.2 nM) Au NPs [16], show size-dependent biocompatibility and toxicity of the Au NPs on embryonic development.

time, in order to understand their physicochemical-dependent nanotoxicity and rationally design biocompatible nanomaterials. It is worth noting that the conclusions reported in this study are specific for the sizes and shapes of the NPs used in this study, and cannot be generally applied to other NPs or extrapolated to other sizes of Au NPs. In other words, size- and chemical-dependent biocompatibility and toxicity of Au and Ag NPs may not be linear, and further studies would be needed. Our studies suggest that it is very likely that each size of the Au or Ag NPs possesses its own properties.

Taken together, these important findings offer interesting new insights into the size-dependent biocompatibility of Au NPs, and chemical-dependent nanotoxicity of Au and Ag NPs at single NP resolution. Such studies are essential for rational design of biocompatible nanomaterials for a wide range of applications, including *in vivo* imaging, drug delivery and implant devices. For example, the smaller NPs could more easily penetrate into the sub-compartments of living organisms to enable *in vivo* imaging and sensing for effective diagnosis, while the larger NPs could carry a larger payload of therapeutic agents to enable effective drug delivery and achieve effective therapy. We have demonstrated that DFOMS-MSIS is a powerful imaging tool for real-time *in vivo* imaging of transport and the effects of single Au NPs, and for quantitative

analysis of individual Au NPs embedded in the tissues. This study further demonstrates that LSPR spectra of single Au NPs can be used to study size-dependent biocompatibility and nanotoxicity. One can now use the similar approaches, such as single NP fluorescence or Raman spectroscopy, to study the transport and toxicity of nanomaterials with given optical and spectral properties.

## 2.7. Summary

In summary, we have synthesized and characterized purified and stable (non-aggregated) Au NPs ( $86.2 \pm 10.6$  nm) and developed DFOMS-MSIS to study their transport into/in embryos and their effects on embryonic development *in vivo* in real-time at single NP resolution. We found that single Au NPs passively diffused into the CS of the embryos via their chorionic pore canals and continued into the IME. The diffusion coefficients of single Au NPs range from  $1.7 \times 10^{-9}$  to  $6.3 \times 10^{-9}$  cm<sup>2</sup> s<sup>-1</sup>, as single Au NPs passively diffuse through different locations of the developing embryos, suggesting diverse viscosity gradients and transport barriers within the embryos. The majority of embryos (96%) that are chronically incubated with the Au NPs (0–20 pM) over 120 h develop into normal zebrafish, while insignificant amounts of embryos either die (3%) or develop into deformed zebrafish (1%), which are independent of the dose of Au NPs. The Au NPs are embedded in various tissues of normal and deformed zebrafish, and more Au NPs are observed in the deformed ones. The results show that the Au NPs diffuse into the embryos and stay inside the embryos throughout their development (120 h), and random walk of single Au NPs may be attributed to their stochastic toxic effects on embryonic development. By comparing with our previous study of smaller Au NPs ( $11.6 \pm 0.9$  nm) and various-sized Ag NPs ( $11.6 \pm 3.5$ ;  $41.6 \pm 9.1$ ; and  $95.4 \pm 16.0$  nm), we found the size-dependent biocompatibility of Au NPs and chemical-dependent biocompatibility and nanotoxicity of Au and Ag NPs. At the same given doses, the larger Au NPs ( $86.2 \pm 10.6$  nm) are slightly more biocompatible with embryonic development than the smaller Au NPs ( $11.6 \pm 0.9$  nm), while the similar-sized Ag NPs are much more toxic than the Au NPs. Note that we observe similar diffusion coefficients of the same sizes of Ag and Au NPs into/in embryos. Thus, the size-dependent biocompatibility of the Au NPs is very unlikely to be attributable to their size-dependent accumulation inside the embryos. Taken together, this study offers new tools and new insights for the study of transport and toxicity of Au NPs *in vivo* in real-time at single NP resolution, which are essential to the rational design of biocompatible NPs for a wide variety of biomedical applications, including *in vivo* imaging, drug delivery and implant devices.

## 3. Materials and methods

### 3.1. Synthesis and characterization of stable and purified Au NPs ( $86.2 \pm 10.8$ nm)

We synthesized the Au NPs ( $86.2 \pm 10.8$  nm) by reducing a freshly prepared HAuCl<sub>4</sub> solution (520 ml, 0.01% w/v, in DI water) with a freshly prepared sodium citrate solution (2.2 ml, 1.1% w/v) [33–35]. The HAuCl<sub>4</sub> in a three-necked round bottom flask was heated to the boiling temperature (100°C) under refluxing and stirring, and the sodium citrate solution

was rapidly added into the flask. After the colour of the solution changed from yellow to colourless, to dark purple and finally to dark red, we continued stirring and refluxing the solution for another 15 min. We then stopped heating the solution until it cooled to room temperature. The NPs were immediately filtered using 0.22 µm filters, and washed three times with DI water (18 MΩ, Barnstead) using centrifugation to remove the by-products and any excess chemicals from NP synthesis.

We first spun down the NPs using centrifugation (1000 rpm, DYNAC II, Clay Adams, 1 h). We imaged the supernatant using DFOMS to ensure that there were no NPs in the supernatant (all of the NPs were spun down). If we found that any single NPs were present in the supernatant, we would increase the speed or time of centrifugation or use an ultra-centrifugation system (Beckman L90) to remove them from the supernatant. We then removed the supernatant, and resuspended the NPs (pellet) in DI water via vortex. We repeated such a washing step three times. The supernatant removed from the last washing step was collected and used to incubate with embryos over 120 h, which served as a control experiment to determine the effects of any possible trace chemicals involved in NP synthesis on embryonic development. All chemicals were purchased from Sigma and used as received, and the DI water was used to prepare solutions and rinse glassware.

We resuspended the pellet of the purified Au NPs in egg water and characterized their sizes, concentrations and optical properties over 120 h to determine their stability using high-resolution TEM (JEOL, JEM-2100 F), DLS (Nicomp 380ZLS particle sizing system), UV-vis spectroscopy (Hitachi U2010) and DFOMS (figures 1 and 2), respectively. The TEM samples were prepared by adding one drop of Au NP suspension (5 µl) onto each TEM grid, which was dried rapidly. We repeated such a process two or three times to ensure that each TEM grid was covered with sufficient Au NPs for effective TEM imaging (figure 1A,B). For DLS measurements (figure 1C), the average sizes of the NPs (20 pM, 700 µl of Au NPs suspended in egg water in a borosilicate tube) were measured seven times at each given time over 120 h at room temperature using DLS (ensemble measurement). The purified and stable Au NPs were used for probing of their diffusion into embryos and for studying their effects on embryonic development over 120 h.

For DFOMS measurements (figure 2), we sampled the Au NPs suspended in egg water into a home-made microchamber, and directly acquired LSPR spectra (colours) and the number of single Au NPs in the microchamber in real-time using DFOMS, as we described previously [7–22]. Histograms of plasmonic spectra (colours) of single Au NPs in egg water at each given time (figure 2C) were correlated with the sizes of single Au NPs measured by TEM, because TEM samples were prepared from the same Au NP samples in egg water at the same given incubation time. We have fully described the designs and applications of our DFOMS for real-time imaging and spectroscopic characterization of single NPs in solutions, single live cells and embryos, and for single molecule detection [7–22]. In this study, a dark-field microscope coupled with a CCD camera (EMCCD or Coolsnap HQ2) and a spectrograph (Spectra Pro-150, Roper Scientific), or MSIS (N-MSI-VIS-FLEX, CRi, Hopkinton, MA, USA) are used to image and characterize LSPR spectra of single Ag NPs. The MSIS is an integrated system of a CCD camera (SonyICX 285) and a liquid crystal tunable filter [17–19,22,41,42]. DFOMS-MSIS can simultaneously acquire dark-field plasmonic optical images and spectra of massive amounts of individual NPs with a spectral resolution of 1 nm, and enable high-throughput spectral analysis and characterization of single NPs. The dark-field microscope is equipped with a dark-field condenser (oil, 1.43–1.20), a microscope illuminator (halogen lamp, 100 W) and a 100× objective (plan fluor 100×, NA 0.5–1.3, oil), as we described previously [7–22].

### 3.2. Breeding and monitoring of development of zebrafish embryos

We housed wild-type adult zebrafish (Aquatic Ecosystems) in a stand-alone system (Aquatic Habitats), and maintained and bred zebrafish as described previously [11,16,18,19,43]. Briefly, we placed two pairs of mature zebrafish into a clean 10 gallon breeding tank, and used a light (14 h)–dark (10 h) cycle to trigger breeding and fertilization of embryos. We collected the embryos at 2 hpf, transferred them into a Petri dish, and rinsed them well with egg water to remove the surrounding debris. The washed embryos were then used for real-time imaging of the diffusion and transport of single Au NPs into/in embryos and for the quantitative study of their effects on embryonic development.

### 3.3. *In vivo* real-time imaging of diffusion and transport of single Au NPs into/in embryos

We incubated the cleavage-stage embryos with the purified Au NPs (20 pM) in home-made imaging microchambers, and imaged the diffusion of single Au NPs into embryos in real-time using our DFOMS (figures 3 and 4). Distinctive plasmonic optical properties (colours) of single Au NPs enable them to be distinguished from embryonic debris and zebrafish tissues, which appear white under dark-field illumination. LSPR spectra of single Au NPs were acquired by DFOMS–MSIS (figure 2E), as we described previously [7,11,16–19,22,36,42].

### 3.4. Study of dose-dependent biocompatibility and toxicity of Au NPs ( $86.2 \pm 10.8$ nm)

We incubated the cleavage-stage embryos with a dilution series of the purified Au NPs (2.0 ml per well of 0, 0.66, 1.3, 2.4, 5.1, 9.9 and 20 pM or 0, 2.6, 5.1, 9.5, 20, 39 and 78  $\mu\text{g ml}^{-1}$ ) in 24-well plates (four embryos per well) for 120 h. The molar concentrations of Au NPs were calculated as we described previously [11,16,18,19,35]. We conducted the control experiments by incubating the embryos (four embryos per well) with egg water alone (in the absence of NPs) and the supernatants collected from washing Au NPs (dispersed in egg water with the same dilution factors as those prepared for Au NPs in egg water) in two rows of the same well plate as those embryos incubated with the NPs. Four replicates (three additional sets of four embryos at each given concentration in each well) were performed simultaneously. Thus, the 16 embryos in three wells for each concentration and the control were studied for each run of the experiment. Each experiment was carried out at least three times, and a total minimal number of 48 embryos (12 replicates of four embryos for each concentration) were studied for each NP concentration and each control experiment to gain representative statistics (figure 5).

The microwell plates were incubated in a water bath at 28.5°C under dark for 120 h. The developing embryos in the plates were

imaged at 2, 24, 48, 72, 96 and 120 hpf, using an inverted microscope (Zeiss Axiovert) equipped with a CCD camera (CoolSnap, Roper Scientific).

### 3.5. Quantitative imaging of single Au NPs embedded in individual zebrafish

The cleavage-stage embryos were incubated with given concentrations (0–20 pM) of the Au NPs continuously (chronically) for 120 h, and developed to normal or deformed zebrafish. We then rinsed the zebrafish with DI water to remove any external NPs, fixed the zebrafish using a tissue processor (Microm STP-120 spin, Thermo Fisher Scientific), and sectioned them to prepare ultra-thin tissue samples (1–4  $\mu\text{m}$  thickness) using a microtome (HM360 rotary microtome, Thermo Fisher Scientific), as we described previously [11,16,18,19]. The number and sizes of individual Au NPs embedded in the tissues of interest were quantitatively determined using their size-dependent LSPR spectra acquired by DFOMS–MSIS (figures 6 and 7). A minimum of three slices of each given tissue were analysed for each measurement.

### 3.6. Statistical analysis

For characterization of sizes, shapes, LSPR spectra, and stability of single Au NPs, we studied 300 individual Au NPs for each sample with a minimum of 100 NPs for each measurement. For real-time imaging of transport and diffusion of single Au NPs into and in embryos, we investigated a minimum of 12 embryos for each given concentration with four embryos per measurement. For each NP concentration and each control experiment to study the dose-dependent effects of the Au NPs on embryonic development, we characterized a total minimal number of 48 embryos with 12 replicates of four embryos per measurement.

Using a conventional statistical analysis method (ANOVA), we analysed the differences of the percentages of embryos that developed to normal or deformed zebrafish, or that became dead, as they were incubated with various concentrations of the Au NPs (0–20 pM), and found insignificant dose-dependent nanotoxicity with a confidence level of 95% ( $p = 0.05$ ). Notably, we characterized the effects of Au NPs on embryonic development at single embryo and single NP resolutions. These approaches enable us to observe the rare events of interest (few deformed zebrafish in figure 5B), which otherwise would be buried under ensemble measurements. The study of a large number of single Au NPs and single embryos offers sufficient statistics to depict the ensemble properties of NPs and their effects on embryonic development at single NP and single embryo resolutions.

This study is supported in part by the NSF (NIRT: CBET 0507036) and NIH (R01 GM076440; 3R01-GM076440-04S1). L.M.B. is grateful for the support of NIH-GRAS (3R01-GM076440-01S1).

## References

- Bohren CF, Huffman DR. 1983 *Absorption and scattering of light by small particles*, pp. 287–380. New York, NY: Wiley.
- Kreibig U, Vollmer M. 1995 *Optical properties of metal clusters*, pp. 14–123. Berlin, Germany: Springer.
- Mie G. 1908 Beitrag zur optik trüber medien, speziell kolloidaler metralösungen. *Annu. Phys.* **25**, 377–445. (doi:10.1002/andp.19083300302)
- Kelly KL, Coronado E, Zhao LL, Schatz GC. 2003 The optical properties of metal nanoparticles: the influence of size, shape, and dielectric environment. *J. Phys. Chem. B* **107**, 668–677. (doi:10.1021/jp026731y)
- Mulvaney P. 1996 Surface plasmon spectroscopy of nanosized metal particles. *Langmuir* **12**, 788–800. (doi:10.1021/la9502711)
- Lee KS, El-Sayed MA. 2006 Gold and silver nanoparticles in sensing and imaging: sensitivity of plasmon response to size, shape, and metal composition. *J. Phys. Chem. B* **110**, 19 220–19 225. (doi:10.1021/jp062536y)
- Nallathamby PD, Huang T, Xu X-HN. 2010 Design and characterization of optical nano rulers of single nanoparticles using optical microscopy and spectroscopy. *Nanoscale* **2**, 1715–1722. (doi:10.1039/c0nr00303d)

8. Huang T, Nallathamby PD, Gillet D, Xu X-HN. 2007 Design and synthesis of single nanoparticle optical biosensors for imaging and characterization of single receptor molecules on single living cells. *Anal. Chem.* **79**, 7708–7718. (doi:10.1021/ac0709706)
9. Huang T, Nallathamby PD, Xu X-HN. 2008 Photostable single-molecule nanoparticle optical biosensors for real-time sensing of single cytokine molecules and their binding reactions. *J. Am. Chem. Soc.* **130**, 17 095–17 105. (doi:10.1021/ja8068853)
10. Lee KJ, Browning LM, Huang T, Ding F, Nallathamby PD, Xu X-HN. 2010 Probing of multidrug ABC membrane transporters of single living cells using single plasmonic nanoparticle optical probes. *Anal. Bioanal. Chem.* **397**, 3317–3328. (doi:10.1007/s00216-010-3864-8)
11. Lee KJ, Nallathamby PD, Browning LM, Osgood CJ, Xu X-HN. 2007 *In vivo* imaging of transport and biocompatibility of single silver nanoparticles in early development of zebrafish embryos. *ACS Nano* **1**, 133–143. (doi:10.1021/nn700048y)
12. Nallathamby PD, Lee KJ, Desai T, Xu X-HN. 2010 Study of multidrug membrane transporters of single living *Pseudomonas aeruginosa* cells using size-dependent plasmonic nanoparticle optical probes. *Biochemistry* **49**, 5942–5953. (doi:10.1021/bi100268k)
13. Nallathamby PD, Lee KJ, Xu X-HN. 2008 Design of stable and uniform single nanoparticle photonics for *in vivo* dynamics imaging of nanoenvironments of zebrafish embryonic fluids. *ACS Nano* **2**, 1371–1380. (doi:10.1021/nn800048x)
14. Xu X-HN, Brownlow WJ, Kyriacou SV, Wan Q, Viola JJ. 2004 Real-time probing of membrane transport in living microbial cells using single nanoparticle optics and living cell imaging. *Biochemistry* **43**, 10 400–10 413. (doi:10.1021/bi036231a)
15. Xu X-HN, Chen J, Jeffers RB, Kyriacou SV. 2002 Direct measurement of sizes and dynamics of single living membrane transporters using nano-optics. *Nano Lett.* **2**, 175–182. (doi:10.1021/nl015682i)
16. Browning LM, Lee KJ, Huang T, Nallathamby PD, Lowman J, Xu X-HN. 2009 Random walk of single gold nanoparticles in zebrafish embryos leading to stochastic toxic effects on embryonic developments. *Nanoscale* **1**, 138–152. (doi:10.1039/b9nr00053d)
17. Huang T, Browning LM, Xu X-HN. 2012 Far-field photostable optical nanoscopy (PHOTON) for real-time super-resolution single-molecular imaging of signaling pathways of single live cells. *Nanoscale* **4**, 2797–2812. (doi:10.1039/c2nr11739h)
18. Lee KJ, Browning LM, Nallathamby PD, Desai T, Cherukui P, Xu X-HN. 2012 *In vivo* quantitative study of size-dependent transport and toxicity of single silver nanoparticles using zebrafish embryos. *Chem. Res. Toxicol.* **25**, 1029–1046. (doi:10.1021/tx300021u)
19. Lee KJ, Nallathamby PD, Browning LM, Desai T, Cherukui P, Xu X-HN. 2012 Single nanoparticle spectroscopy for real-time *in vivo* quantitative analysis of transport and toxicity of single nanoparticles in single embryos. *Analyst* **137**, 2973–2986. (doi:10.1039/c2an35293a)
20. Nallathamby PD, Xu X-HN. 2010 Study of cytotoxic and therapeutic effects of stable and purified silver nanoparticles on tumor cells. *Nanoscale* **2**, 942–952. (doi:10.1039/c0nr00080a)
21. Kyriacou SV, Brownlow WJ, Xu XHN. 2004 Using nanoparticle optics assay for direct observation of the function of antimicrobial agents in single live bacterial cells. *Biochemistry* **43**, 140–147. (doi:10.1021/bi0351110)
22. Huang T, Xu X-HN. 2011 Multicolored nanometer-resolution mapping of single protein-ligand binding complex using far-field photostable optical nanoscopy (PHOTON). *Nanoscale* **3**, 3567–3572. (doi:10.1039/c1nr10182j)
23. Murphy CJ, Gole AM, Stone JW, Sisco PN, Alkiliary AM, Goldsmith EC, Baxter SC. 2008 Gold nanoparticles in biology: beyond toxicity to cellular imaging. *Acc. Chem. Res.* **41**, 1721–1730. (doi:10.1021/ar800035u)
24. Dreaden EC, El-Sayed MA. 2012 Detecting and destroying cancer cells in more than one way with noble metals and different confinement properties on the nanoscale. *Acc. Chem. Res.* **45**, 1854–1865. (doi:10.1021/ar2003122)
25. Bhattacharya R, Mukherjee P. 2008 Biological properties of ‘naked’ metal nanoparticles. *Adv. Drug Deliv. Rev.* **60**, 1289–1306. (doi:10.1016/j.addr.2008.03.013)
26. Khlebtsov N, Dykman L. 2011 Biodistribution and toxicity of engineered gold nanoparticles: a review of *in vitro* and *in vivo* studies. *Chem. Soc. Rev.* **40**, 1647–1671. (doi:10.1039/c0cs00018c)
27. Fadeel B, Garcia-Bennett AE. 2010 Better safe than sorry: understanding the toxicological properties of inorganic nanoparticles manufactured for biomedical applications. *Adv. Drug Deliv. Rev.* **62**, 362–374. (doi:10.1016/j.addr.2009.11.008)
28. Fischer HC, Chan WC. 2007 Nanotoxicity: the growing need for *in vivo* study. *Curr. Opin. Biotechnol.* **18**, 565–571. (doi:10.1016/j.copbio.2007.11.008)
29. Hill AJ, Teraoka H, Heideman W, Peterson RE. 2005 Zebrafish as a model vertebrate for investigating chemical toxicity. *Toxicol. Sci.* **86**, 6–19. (doi:10.1093/toxsci/kfi110)
30. Kahn P. 1994 Zebrafish hit the big time. *Science* **264**, 904–905. (doi:10.1126/science.8178149)
31. Teraoka H, Dong W, Hiraga T. 2003 Zebrafish as a novel experimental model for developmental toxicology. *Congenit. Anom. (Kyoto)* **43**, 123–132. (doi:10.1111/j.1741-4520.2003.tb01036.x)
32. Zon LI, Peterson RT. 2005 *In vivo* drug discovery in the zebrafish. *Nat. Rev. Drug Discov.* **4**, 35–44. (doi:10.1038/nrd1606)
33. Handley DA. 1989 Methods for synthesis of colloidal gold. In *Colloid gold: principles, methods and applications* (ed. MA Hayat), pp. 13–29. New York, NY: Academic Press.
34. Turkevich J, Stevenson PC, Hillier J. 1951 A study of the nucleation and growth processes in the synthesis of colloidal gold. *Discuss. Faraday Soc.* **11**, 55–75. (doi:10.1039/d9951100055)
35. Xu X-HN, Huang S, Brownlow W, Salatia K, Jeffers R. 2004 Size and temperature dependence of surface plasmon absorption of gold nanoparticles induced by tris(2,2′-bipyridine)ruthenium(II). *J. Phys. Chem. B* **108**, 15 543–15 551. (doi:10.1021/jp048124b)
36. Huang T, Xu X-HN. 2010 Synthesis and characterization of tunable rainbow colored silver nanoparticle solutions using single-nanoparticle plasmonic microscopy and spectroscopy. *J. Mater. Chem.* **20**, 9867–9876. (doi:10.1039/c0jm01990a)
37. Kusumi A, Sako Y. 1994 Compartmental structure of the plasma membrane for receptor movements as revealed by a nanometer-level motion analysis. *J. Cell Biol.* **125**, 1251–1264. (doi:10.1083/jcb.125.6.1251)
38. Kusumi A, Sako Y, Yamamoto M. 1993 Confined lateral diffusion of membrane receptors as studied by single particle tracking (nanovid microscopy). Effects of calcium-induced differentiation in cultured epithelial cells. *Biophys. J.* **65**, 2021–2040. (doi:10.1016/S0006-3495(93)81253-0)
39. Qian H, Sheetz MP, Elson EL. 1991 Single particle tracking. Analysis of diffusion and flow in two-dimensional systems. *Biophys. J.* **60**, 910–921. (doi:10.1016/S0006-3495(91)82125-7)
40. Tinoco I, Sauer K, Wang J, Puglisi JD. 2002 *Physical chemistry-principles and applications in biological sciences*, pp. 274–290. Englewood Cliffs, NJ: Prentice Hall.
41. Gebhart SC, Thompson RC, Mahadevan-Jansen A. 2007 Liquid-crystal tunable filter spectral imaging for brain tumor demarcation. *Appl. Opt.* **46**, 1896–1910. (doi:10.1364/AO.46.001896)
42. Huang T, Cai W, Elsayed-Ali HE, Xu XHN. 2012 High-throughput ultrasensitive characterization of chemical, structural and plasmonic properties of EBL-fabricated single silver nanoparticles. *Nanoscale* **4**, 380–385. (doi:10.1039/c1nr11368b)
43. Westerfield M. 1993 *The zebrafish book: a guide for the Laboratory use of zebrafish (Danio Rerio\*)*, chs 1–4. Eugene, OR: University of Oregon Press. See [http://zfinfo.org/zf\\_info/zfbook/zfbk.html](http://zfinfo.org/zf_info/zfbook/zfbk.html).